Synthesis of Nano Particles

1. **Spheroids, Clusters and Spheroidal Holoids**
   - **Insulators: Halides, Oxides, Nitrides**
   - **Hard/Strong Matter: Carbons, BN, etc.**
   - **Semiconductors: Chalcogenides**
   - **Metals: Noble Metals, Magnetic Metals**
   - **Organic Matter: Polymers, Biopolymers**
2. **Anisotropic Particles**
   - **Insulators: Halides, Oxides, Nitrides**
   - **Hard/Strong Matter: Carbons, BN, etc.**
   - **Semiconductors: Chalcogenides**
   - **Metals: Noble Metals, Magnetic Metals**
   - **Organic Matter: Polymers, Biopolymers**

Synthesis Routes - Spheroids

R. NESPER ETH ZÜRICH & COLLEGIUM HELVETICUM

1. **Natural (Opal)**
2. **Sol-Gel**
3. **Solvothermal**
4. **Templated**
5. **Hydrolysis**
6. **Extraction**
7. **Flame&Gas Phase**
8. **Phase Transitions**
9. **Corrosion**
10. **Block Structures**
11. **Intercalations**

Bending of a layer

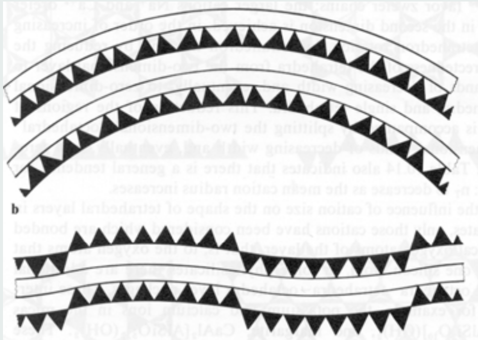

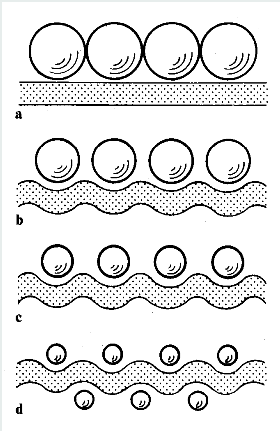

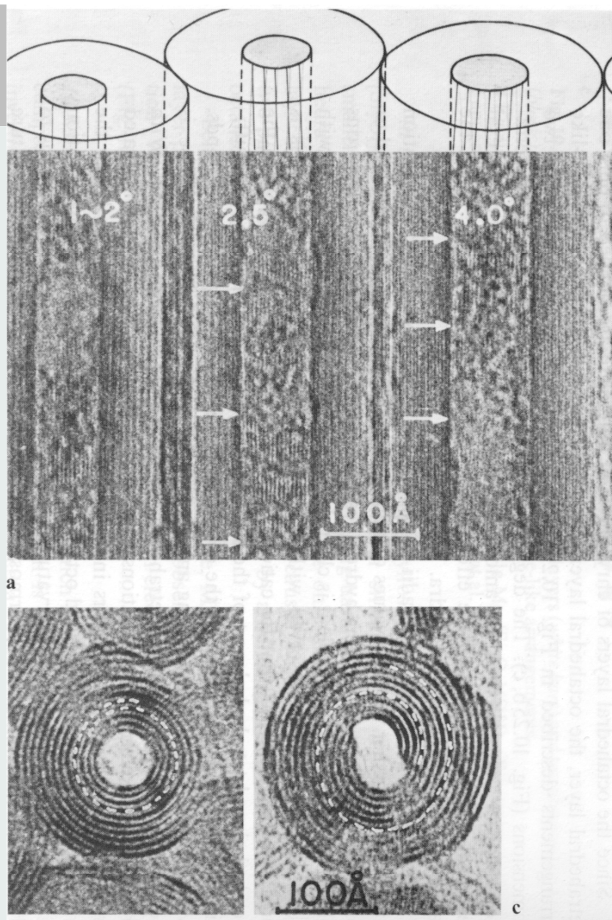

Sigle Layer Misfits - Silicate Minerals

Chrysotile $Mg_3[Si_2O_5](OH)_4$

Anisotropic structure inside layers causes bending of the double layers

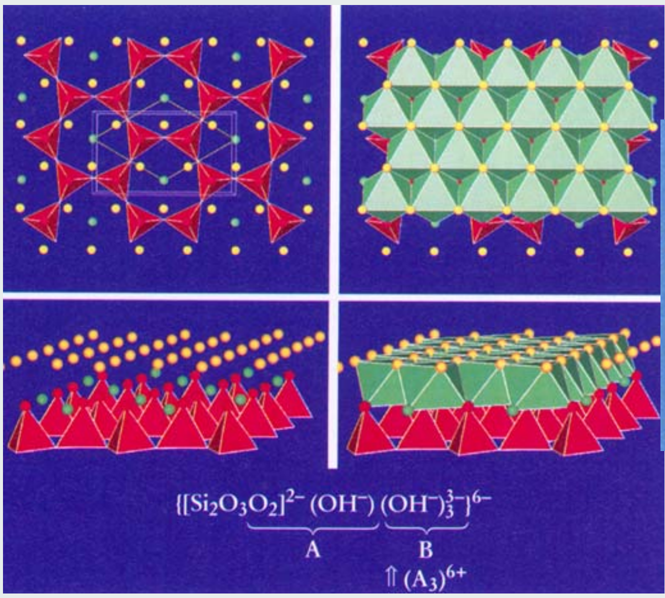

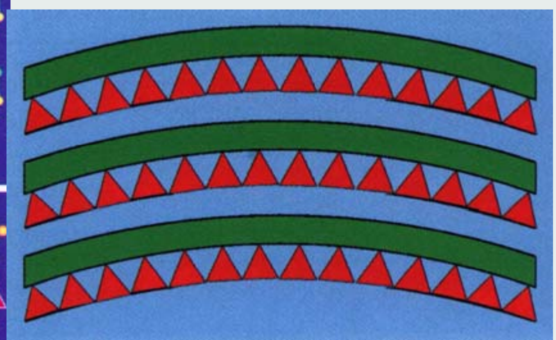

Structure models reproduced from: Röhr, *ChiuZ* 32 (1988) 64

Tubular Silicate Minerals

TEM investigation of the cross-sections of Chrysotile

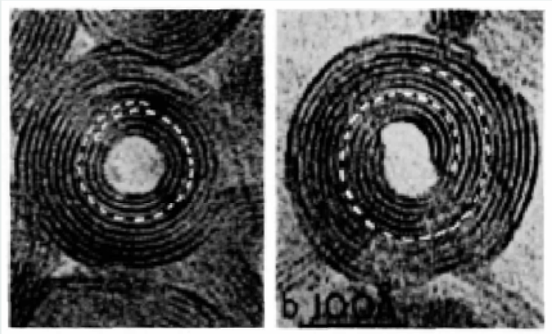

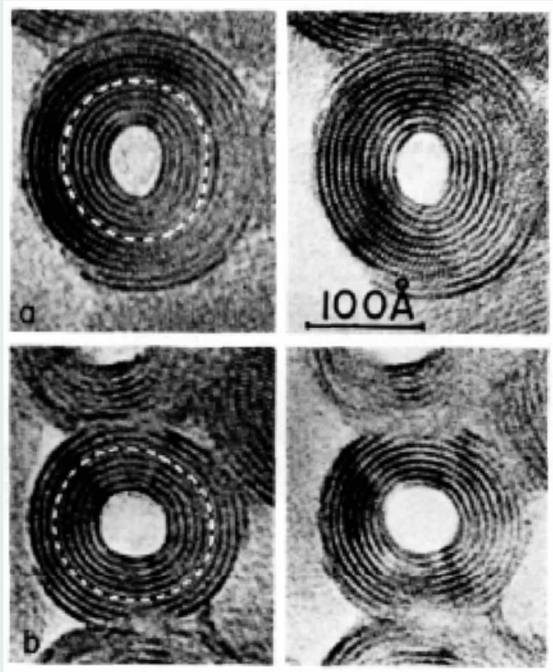

Scrolls of one or more layers

<u>But</u>: also closed, concentric cylinders

Yada, *Acta Crystallogr. A* 27 (1971) 659

Misfit Layer Structures in Ternary Chalcogenides

R. NESPER ETH ZÜRICH & COLLEGIUM HELVETICUM

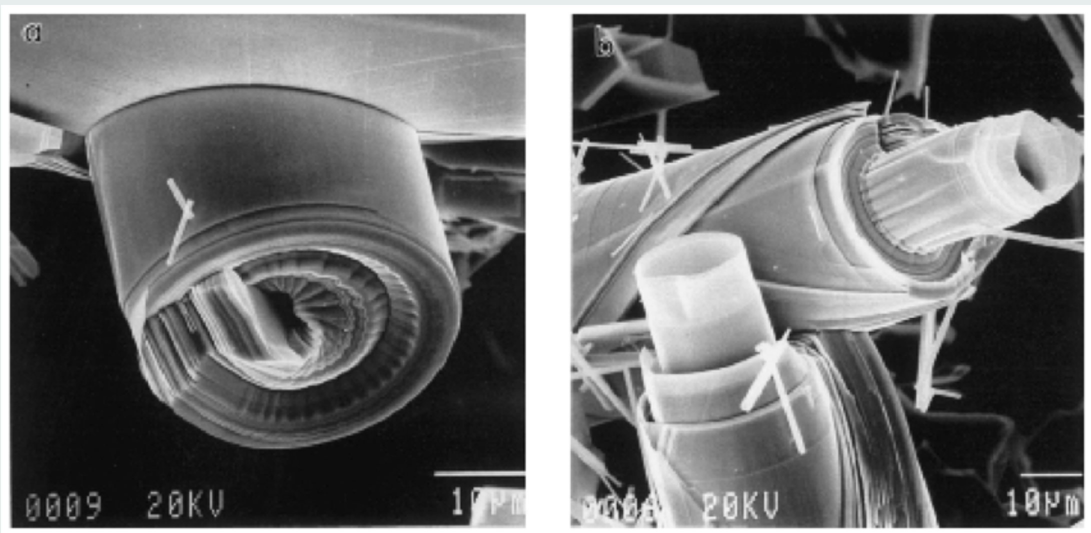

SEM images of tubular crystals in the system Bi-Nb-S

Landa-Cánovas, Gómez-Herrero, Otero-Díaz, *Micron* 32 (2001) 491

Starting from Solids

1. Topotactic reactions
2. Surface reactions
3. Phase widths
4. Intercalations & Ionic exchange

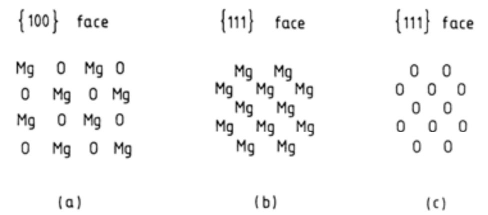

Fig. 2.3 Surface structures of a MgO crystal displaying (a) (100) and (b, c) (111) faces

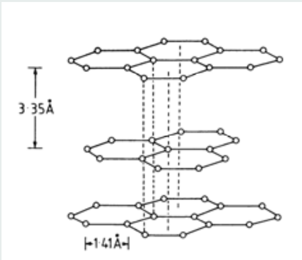

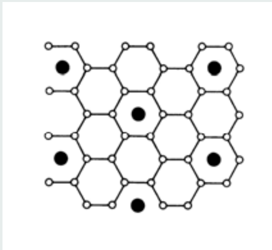

$C_8K \xrightarrow[\text{vacuum}]{\text{partial}} C_{24}K \text{ (steel blue)} \rightarrow C_{36}K \rightarrow C_{48}K \rightarrow C_{60}K$

$\text{Graphite} + H_2SO_4(\text{conc.}) \rightarrow C_{24}{}^+(HSO_4)^- \cdot 2H_2SO_4 + H_2$

$\text{Graphite} + FeCl_3 \rightarrow \text{graphite}/FeCl_3 \text{ intercalate}$

$\text{Graphite} + Br_2 \rightarrow C_8Br$

Topochemical Reactions

Siloxenes

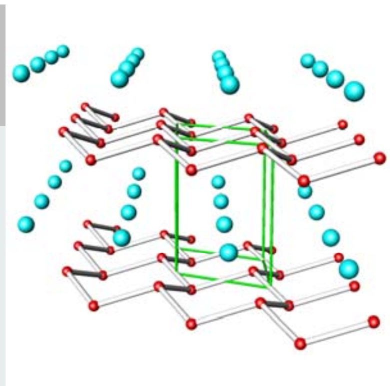

$3CaSi_2 + 6HCl + 3H_2O \rightarrow [Si_6H_3(OH)_3]_n + 3CaCl_2 + 3H_2$

Wöhler 1863 Kautzky 1924

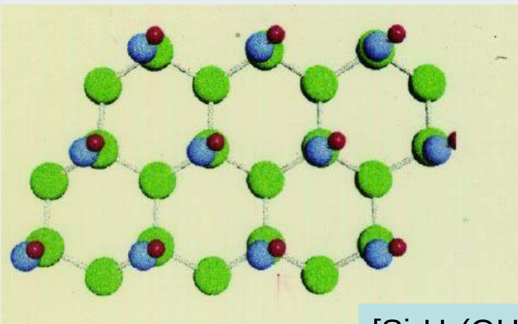

$[Si_6H_3(OH)_3]_n$

2D-poly [1,3,5-tri hydroxy cyclohexa silan]

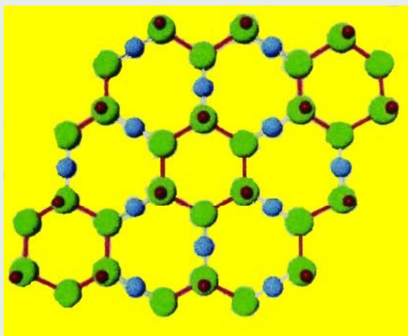

$[Si(OH)]_6O_{6/2}$

Siloxenes

Wöhler 1863

"Das Silicon (= Siloxen) ist lebhaft orangegelb; es besteht aus durchscheinenden gelben Blättchen[..]. Es ist unlöslich in Wasser, in Alkohol, in Kieselchlorid, in Phosphorchlorid, in Schwefelkohlenstoff. Beim Erwärmen wird es vorübergehend tiefer orangegelb. Stärker erhitzt entzündet es sich und verbrennt mit schwacher Verpuffung und Funkensprühen unter Zurücklassung von Kieselsäure, die durch amorphes Silicium braungefärbt ist. Ohne Luftzutritt erhitzt, entwickelt es Wasserstoffgas und hinterläßt ein Gemenge von Kieselsäure und amorphem Silicium in Gestalt glänzender, schwarzbrauner Blättchen. Erst nach vollem Glühen hört die Wasserstoffentwicklung auf. War es mit einer nicht ganz konzentrierten Säure bereitet, so enthält es die weiter unten beschriebene Verbindung beigemengt; es ist dann heller an Farbe und zeigt beim Erhitzen auch in einer Röhre eine Art Verpuffung, unter gleichzeitiger Entwicklung von selbstentzündlichen Kieselwasserstoffgas. Diese Zersetzung des Silicons in der Wärme beginnt schon bei 100 °C[..].

Sehr merkwürdig ist sein Verhalten im Licht. Im Dunkeln bleibt es, selbst im feuchten Zustand, ganz unverändert; im zerstreuten Licht wird es zunehmend blasser und im direkten Sonnenlicht wird es nach kurzer Zeit vollkommen weiß, und zwar unter Entwicklung von Wasserstoffgas. Stellt man es unter Wasser in den Sonnenschein, so fängt es augenblicklich an Wasserstoffgas zu entwickeln, was gleich einer Gährungserscheinung fortdauert, bis es ganz weiß geworden ist [..]. Das Silicon wird weder von Chlor noch rauchender Salpetersäure oder von konzentrierte Schwefelsäure angegriffen, selbst nicht beim Erhitzen damit. Flußsäure erhitzt sich damit; es erhebt sich darin zugleich an die Oberfläche, wird allmählich heller, zuletzt weiß und verschwindet endlich ganz [..]".

Re-detected ~ 1989 !

Intercalation and Delamination

Layered Materials

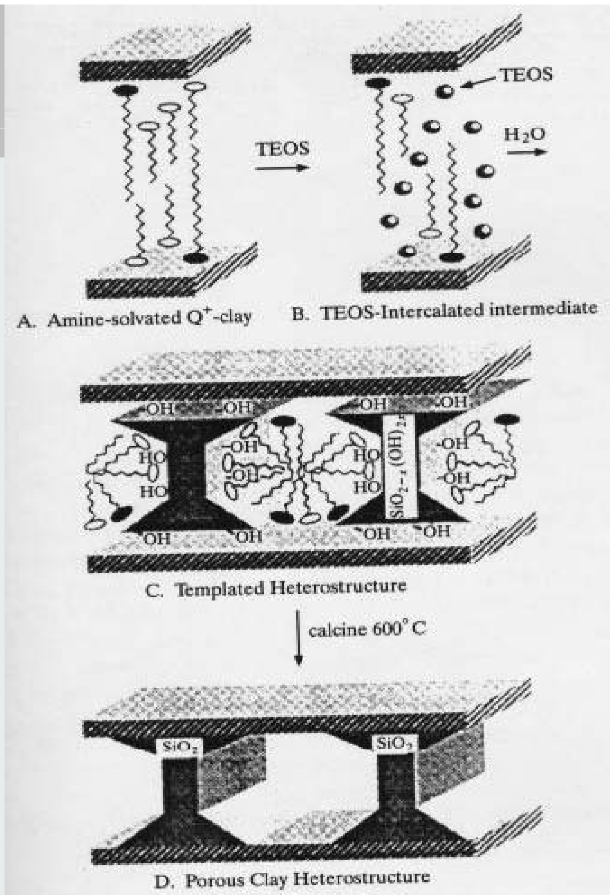

Sol-Gel- Route

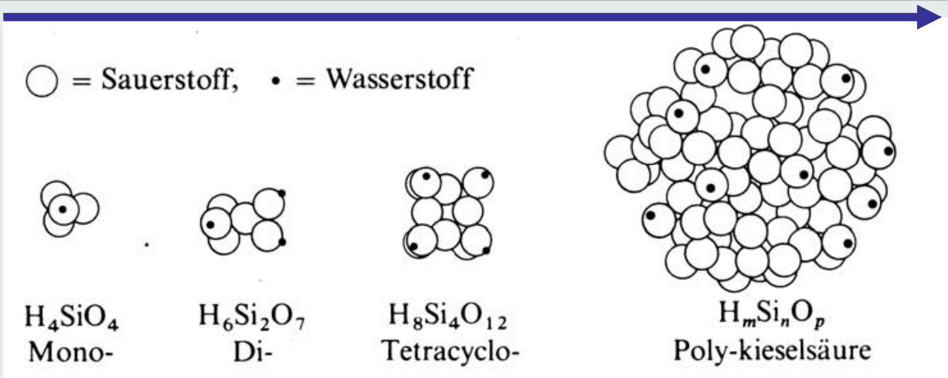

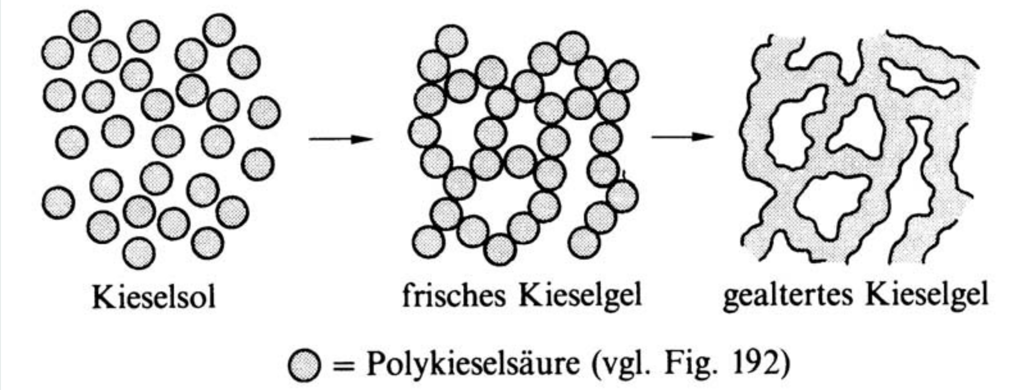

Sol-Gel –Templates as Space Holders and Structure Directors

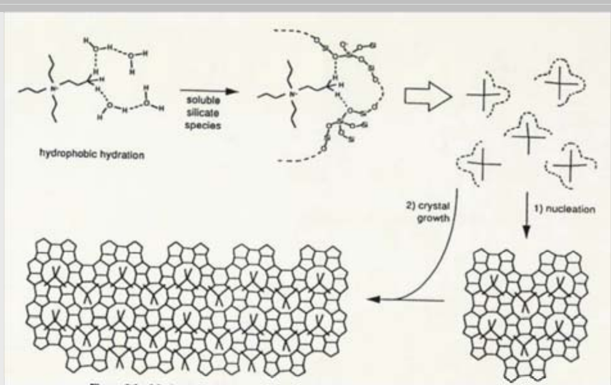

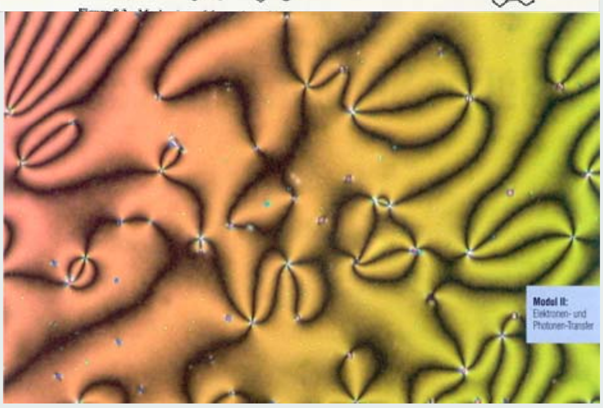

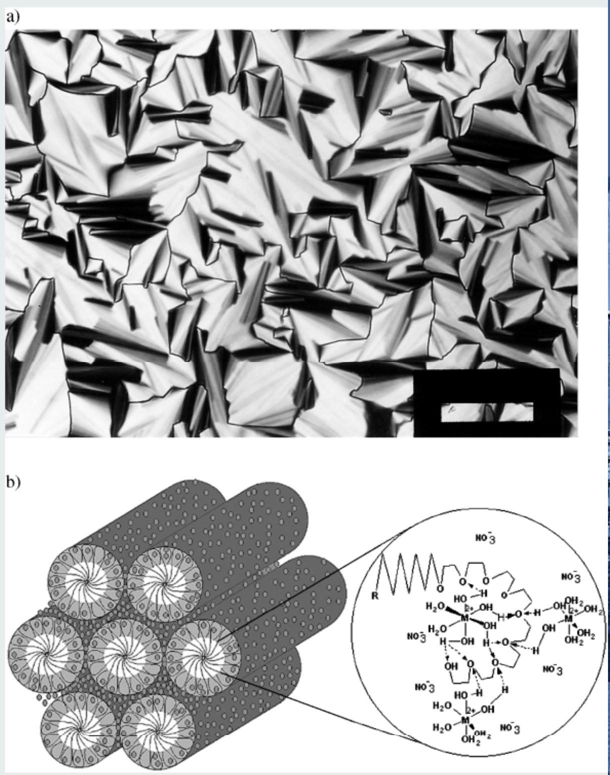

Zeolithes (boiling stones)

concentrations +template + temperature + time + ??

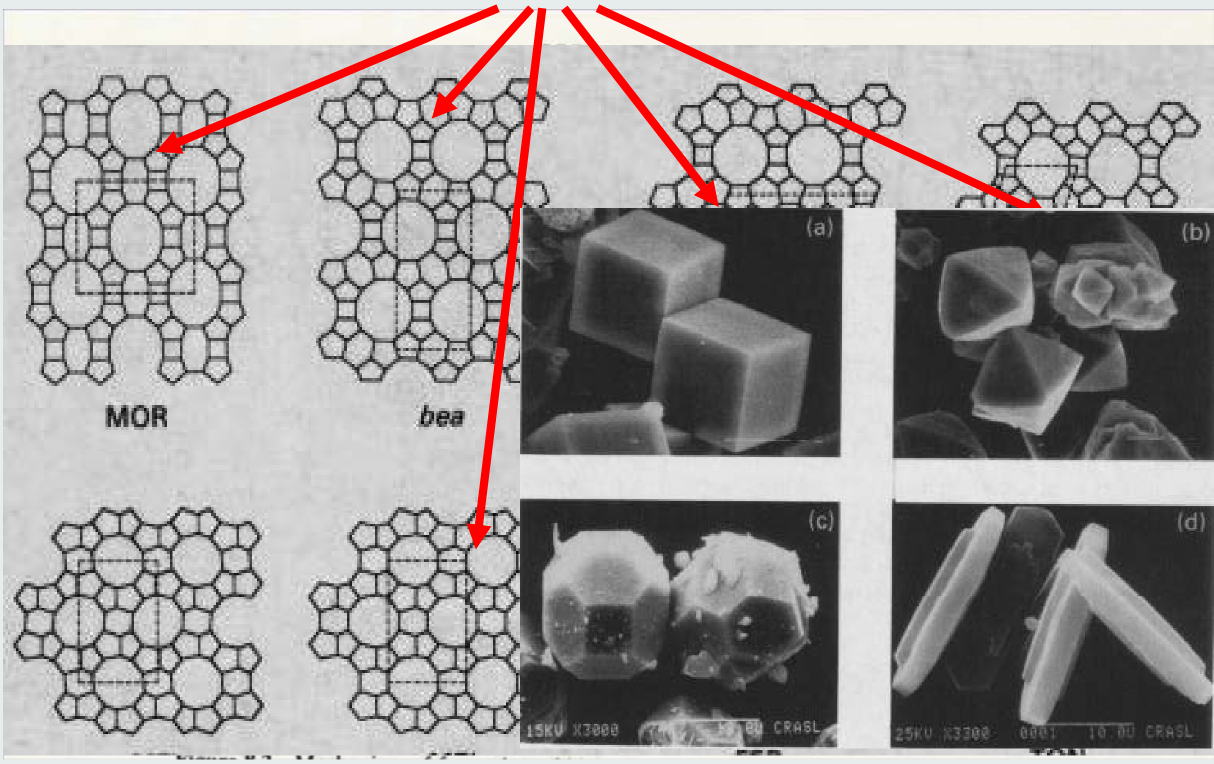

Mesoporous Materials

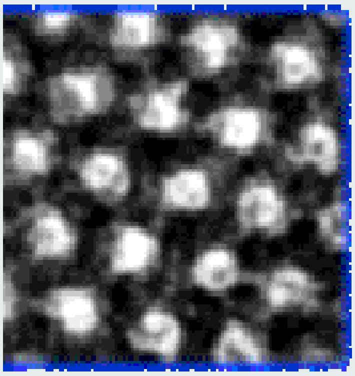

Mesocellular Foams

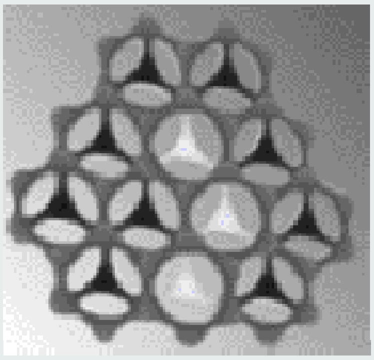

Biomineralization of Silica

Microporous Materials

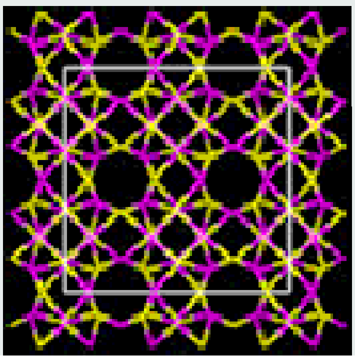

Thermoelectric Materials

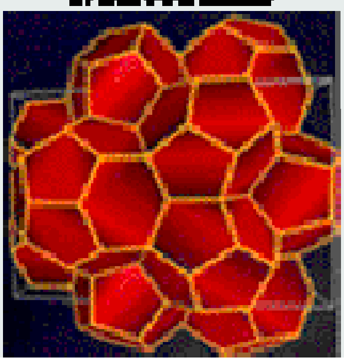

Bi

C

Opals and Photonic Crystals

- **(styrene) nanobeads + TEOS → SiO_2 coated beads**
- **thermalize beads**

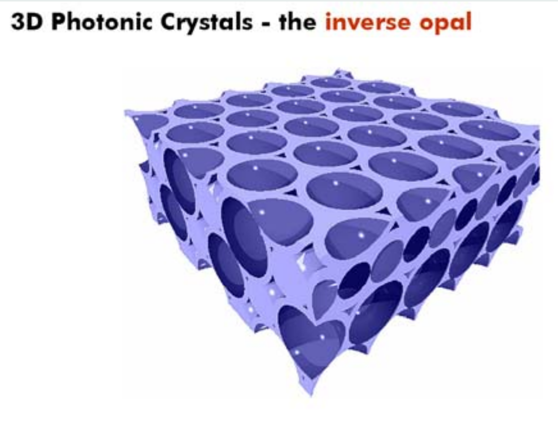

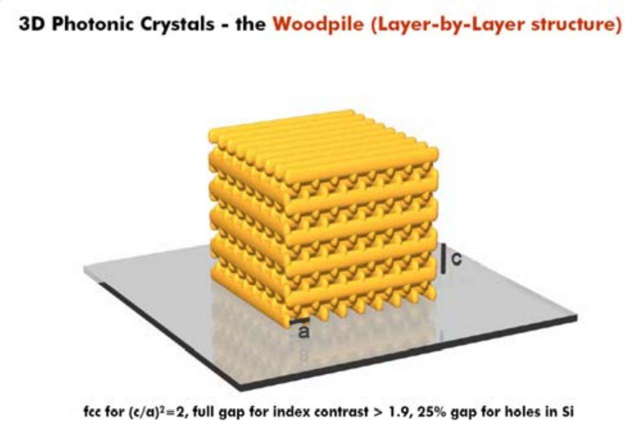

Opals and Photonic Crystals

- **(styrene) nanobeads + TEOS → SiO_2 coated beads**
- **thermalize beads**

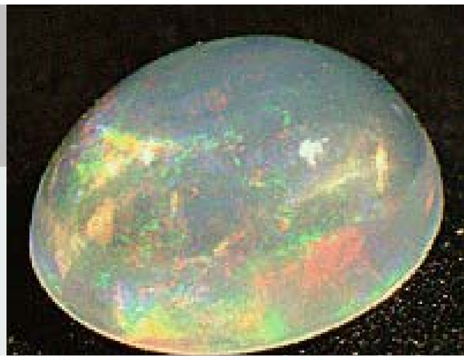

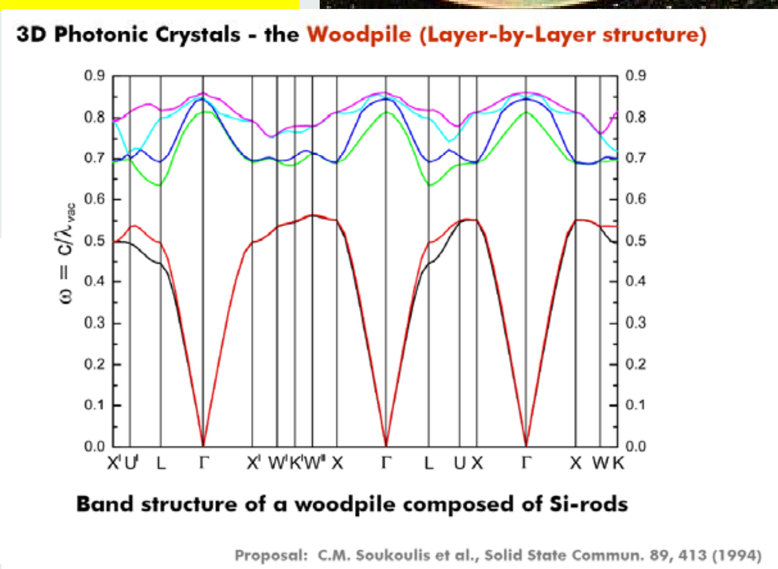

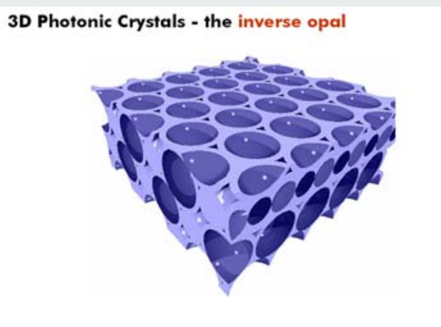

Mesoporous Silicates: MCM41 / MCM48

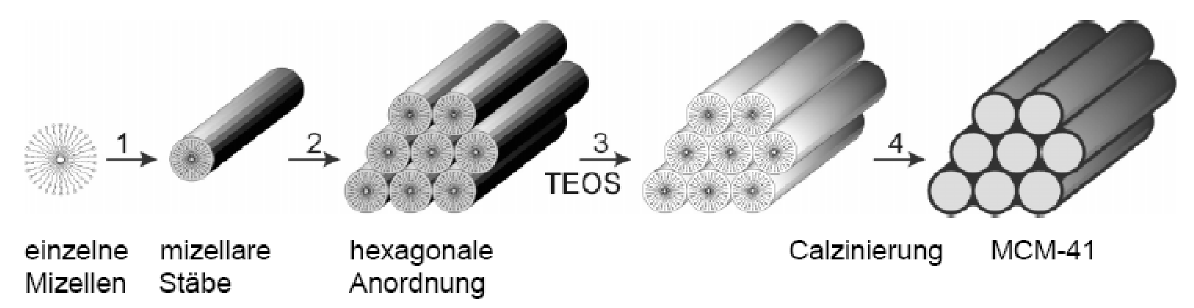

$(C_nH_{2n+1}(CH_3)_3N^+)$

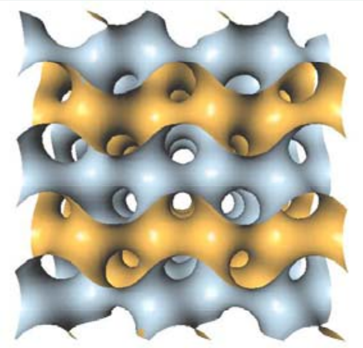

Tetraethoxysilan, TEOS

MCM 41 – hexagonal
Porengrössen 3-8nm

MCM 48 – cubisch
3D-Kanalstruktur

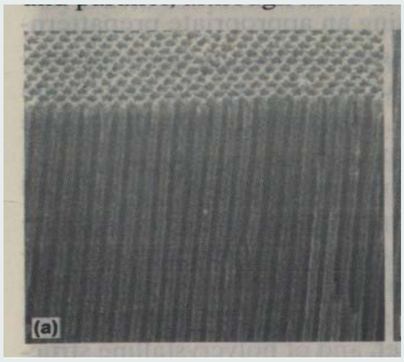

Ionic Liquids

Charakteristic properties:
- low vapour pressure
- thermischal stability
- elektric conductivity
- Phasenseparation from products
- high thermal capacity
- non burning

These liquids are – in contrast to salt melts – not corrosive and thus are used to replace ordinary organic solvents

fields of applications
- **head carrier**
- **Elektrolyte**
- **Analytics**
- **separator**
- **Membran etechniques**

P. Wasserscheid und W. Keim. Angew. Chem. 2000, 112, 3926-3945.

Kationen und Anionen in Ionischen Flüssigkeiten: Ausgewählte Beispiele

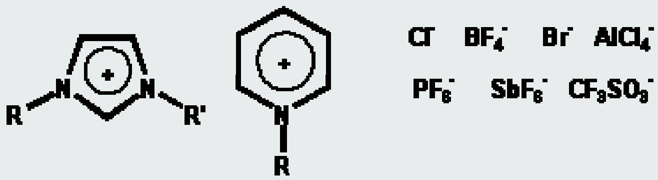

Controlled Precursor Hydrolysis

Polyolate-Route

(ionic liquids

Cu_2O	*ZnO*	*Mn_3O_4*	Al_2O_3	SiO_2	V_2O_5	MoO_3
	CdO		*Bi_2O_3*	SnO_2	Nb_2O_5	WO_3
	CoO		Y_2O_3	*CeO_2*	Ta_2O_5	
			La_2O_3	TiO_2		
			Cr_2O_3	ZrO_2		
			Fe_2O_3			
	Zn_2SiO_4	*$CaTiO_3$*	YVO_4	*$MgAl_2O_4$*	*$ZnNb_2O_6$*	
			MnWO_4	*$BaAl_2O_4$*		
				$CoAl_2O_4$		
				$ZnCo_2O_4$		

(als Ausgangsverbindungen wurden verwendet: $Al(sec\text{-}OC_4H_9)_3$, $Al(OC_3H_7)_3$, $Ba(CH_3COO)_2$, $Bi(CH_3COO)_3$, $Ca(CH_3COO)_2 \cdot xH_2O$, $Cd(CH_3COO)_2 \cdot xH_2O$, $Ce(CH_3COO)_3 \cdot xH_2O$, $Co(CH_3COO)_2 \cdot 4H_2O$, $CrCl_3 \cdot 6H_2O$, $Cu(CH_3COO)_2 \cdot H_2O$, $Fe(CH_3COO)_2$, $La(CH_3COO)_3 \cdot xH_2O$, $Mg(CH_3COO)_2 \cdot 4H_2O$, $Mn(CH_3COO)_2 \cdot 4H_2O$, $Mo(i\text{-}OC_3H_7)_5$, $Nb(OC_2H_5)_5$, $Si(OC_2H_5)_4$, $Sn(C_2H_5)_4$, $Ta(OC_2H_5)_5$, $Ti(OC_2H_5)_4$, $VO(i\text{-}OC_3H_7)_3$, $W(OC_2H_5)_5$, $Y_5O(i\text{-}OC_3H_7)_{13}$, $Y(i\text{-}OC_3H_7)_3$, $Zn(CH_3COO)_2 \cdot 2H_2O$, $Zr(OC_4H_9)_4$)

nanoskaligem V_2O_5

$VO(i\text{-}OC_3H_7)_3$ [mmol]	H_2O [ml]	DEG [ml]	Reaktions-temperatur [°C]	Reaktions-dauer [h]	mittlerer Partikel-durchmesser [nm]
0,5	1	50	180	1	30 bis 40
2,3	2	50	180	2	60 bis 70
5,5	2	50	180	2	90 bis 100
10,6	2	50	190	8	160 bis 180

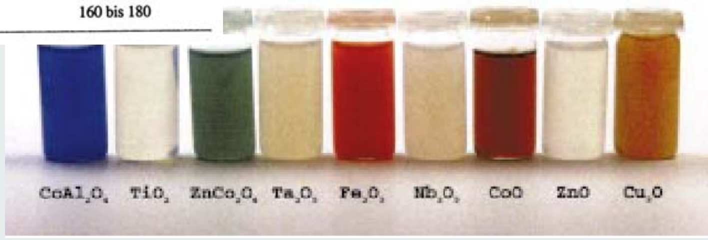

Controlled Precursor Hydrolysis

Polyolate-Route – Particle Size Distribution

Solvent: DEG ($Et(OH)_2$) Metal source : Alkoxides, Halides, T ~ 200 °C

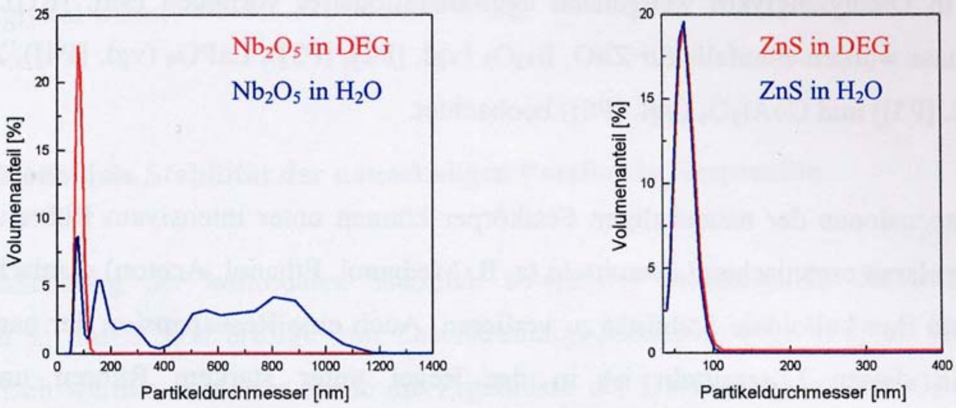

Abb. 4: Partikelgrößenverteilung von nanoskaligem Nb_2O_5 und ZnS in Diethylenglykol sowie nach dem Mischen der DEG-Suspensionen mit Wasser

Polyolate Route – Magnetic Particles – Coating Recipe

$Co(CH_3COO)_2\cdot 4H_2O$/g	$Al(CH_3COO)_2OH$/g	H_2O/ml	DEG/ml	d_{50}/nm
0.50	0.72	1	50	56
2.00	2.86	1	50	96
2.00	2.86	3	50	143

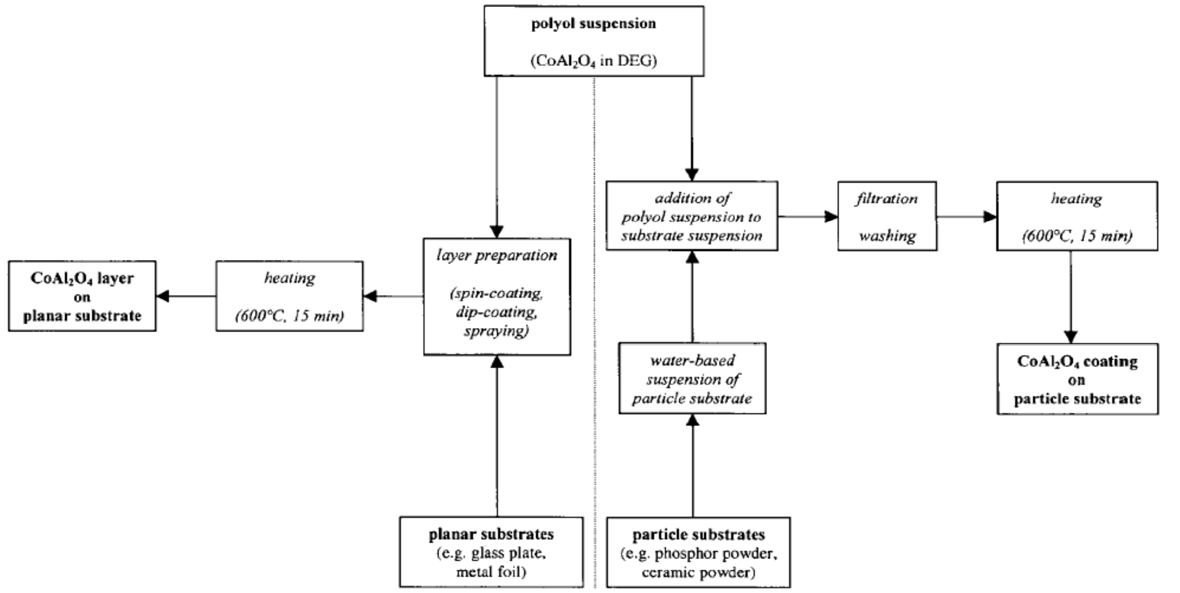

Controlled Precursor Hydrolysis

Metal Organic Precursors

Room-Temperature Organometallic Synthesis of Soluble and Crystalline ZnO Nanoparticles of Controlled Size and Shape

*Miguel Monge, Myrtil L. Kahn, André Maisonnat, and Bruno Chaudret**

Angew. Chem. 2003, 115, 5479–5482

(n-alkylamin)$_2$Zn → ZnO

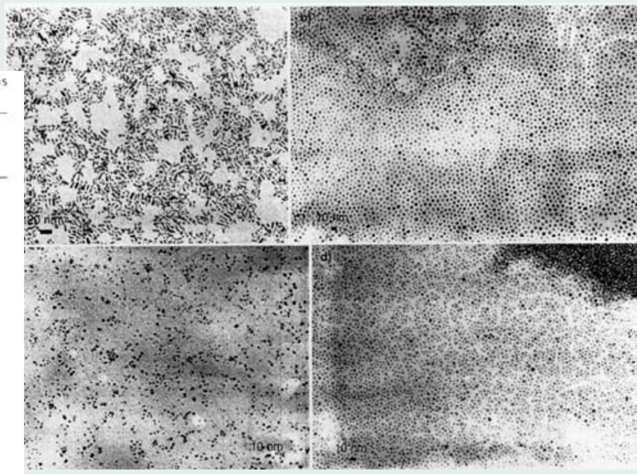

Table 1: Summary of the results obtained after oxidation of the [Zn(c-C$_6$H$_{11}$)$_2$] precursor under various reaction conditions.

Ligand added	Solvent	Time	Overall concentration [M]	Temperature	Size [nm][b]	Morphology
–	THF	Standard[a]	0.042	RT		Agglomerated nanoparticles
HDA	THF	Standard	0.042	RT	8.1 ± 3.3 × 2.6 ± 0.4	Nanorods
HDA	THF	Standard	0.125	RT	11.4 ± 5.7 × 2.8 ± 0.7	Nanorods
HDA	THF	2 weeks	0.042	RT	4.1 ± 0.9	Nanodisks
HDA	THF	Standard	0.042	45 °C	4.8 ± 0.3	Nanodisks
HDA	THF	Standard	0.01	RT	< 3.0 after 1 day 4.3 ± 0.5 after 4 days	Nanodisks
HDA	THF	5 min under Ar	0.042	RT	5.8 ± 1.3 × 2.7 ± 0.3	Nanorods
DDA	THF	Standard	0.042	RT	3.0 ± 0.5	Nanodisks
OA	THF	Standard	0.042	RT	4.0 ± 0.7	Nanodisks
HDA	Toluene	Standard	0.042	RT	4.6 ± 0.9	Nanodisks
HDA	Heptane	Standard	0.042	RT	2.4 ± 0.5	Nanodisks
HDA	–	Standard	–	RT	10.7 ± 1.2 × 1.6 ± 0.3	Nanorods
DDA	–	Standard	–	RT	9.2 ± 2.0 × 3.7 ± 1.8	Nanorods
OA	–	Standard	–	RT	7.4 ± 1.4 × 2.8 ± 0.6	Nanorods
2 HDA	–	Standard	–	RT	~5	Not homogeneous
2 DDA	–	Standard	–	RT	17.1 ± 3.4 × 3.0 ± 0.4	Nanorods
2 OA	–	Standard	–	RT	36.9 ± 10.8 × 2.8 ± 0.3	Nanorods

[a] Standard reaction time is 17 h under Ar and 1 or 2 days of oxidation/evaporation. [b] The values indicate the diameter of nanodisks or the length and width for nanorods; size dispersion is given after the mean size.

Alkoxide Hydrolysis

R. NESPER ETH ZÜRICH & COLLEGIUM HELVETICUM

small needles

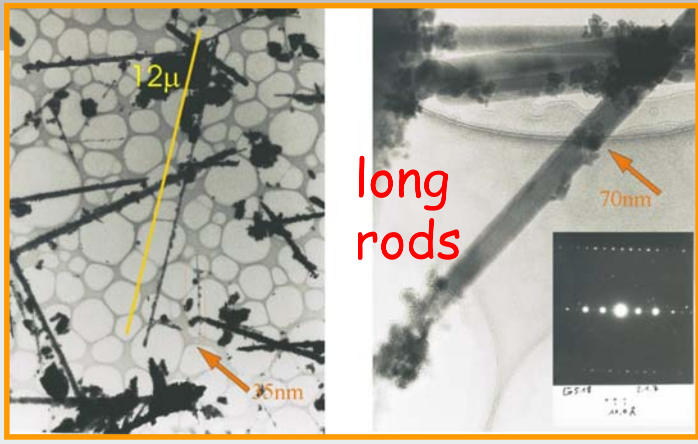

long rods

FeO_x NPs

small rods

large needles

small lenses

large cubes

Hematite-Discs

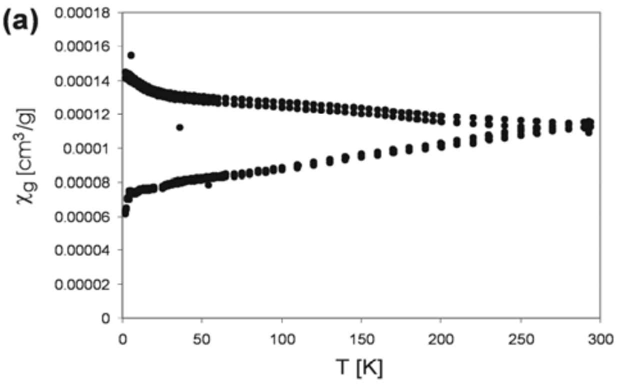

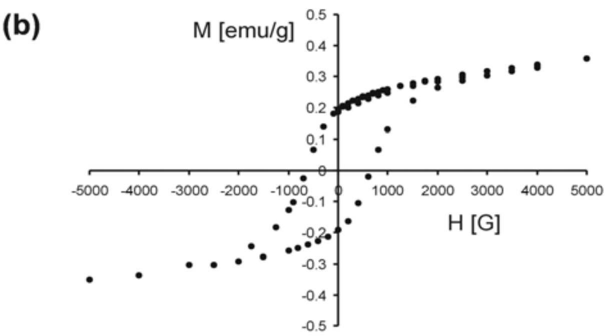

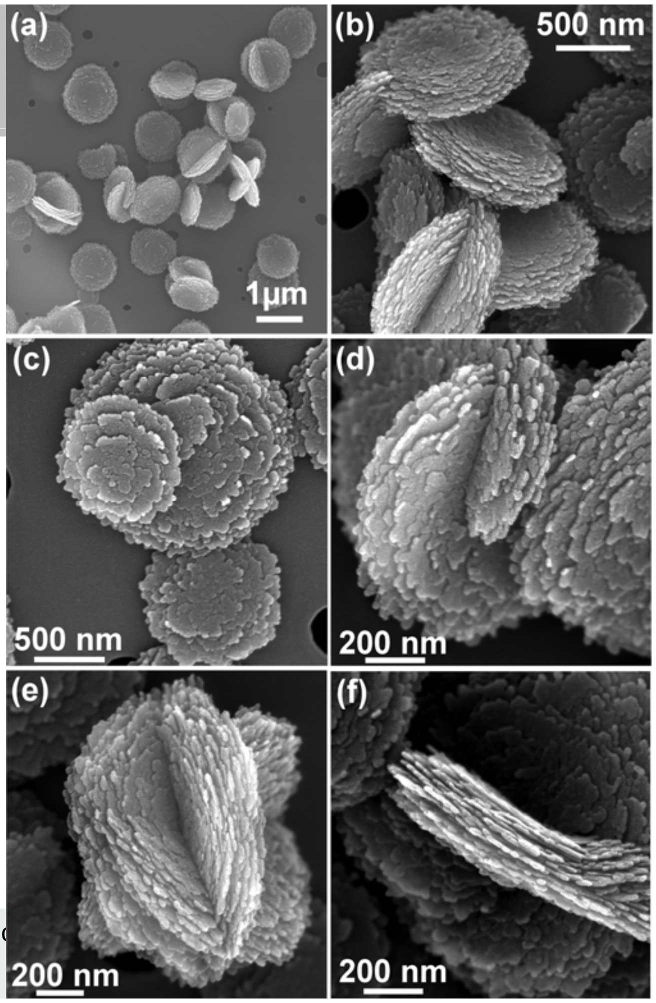

Hematite-Discs

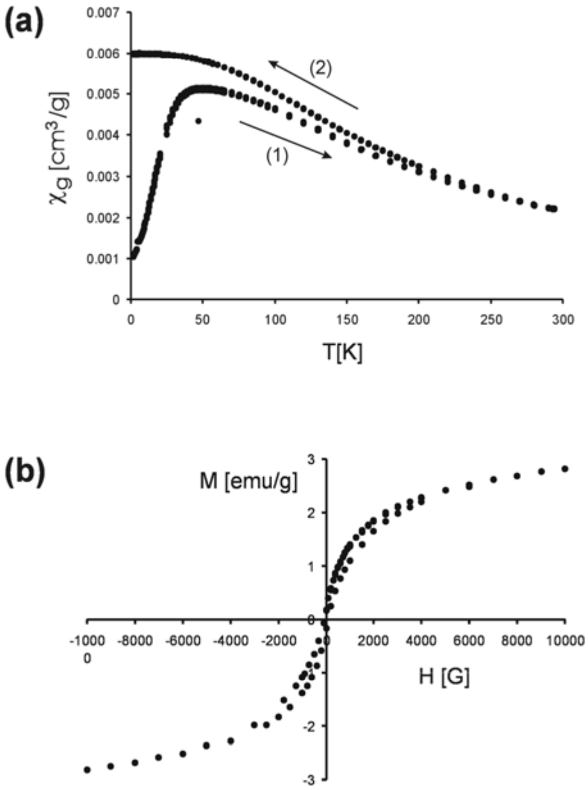

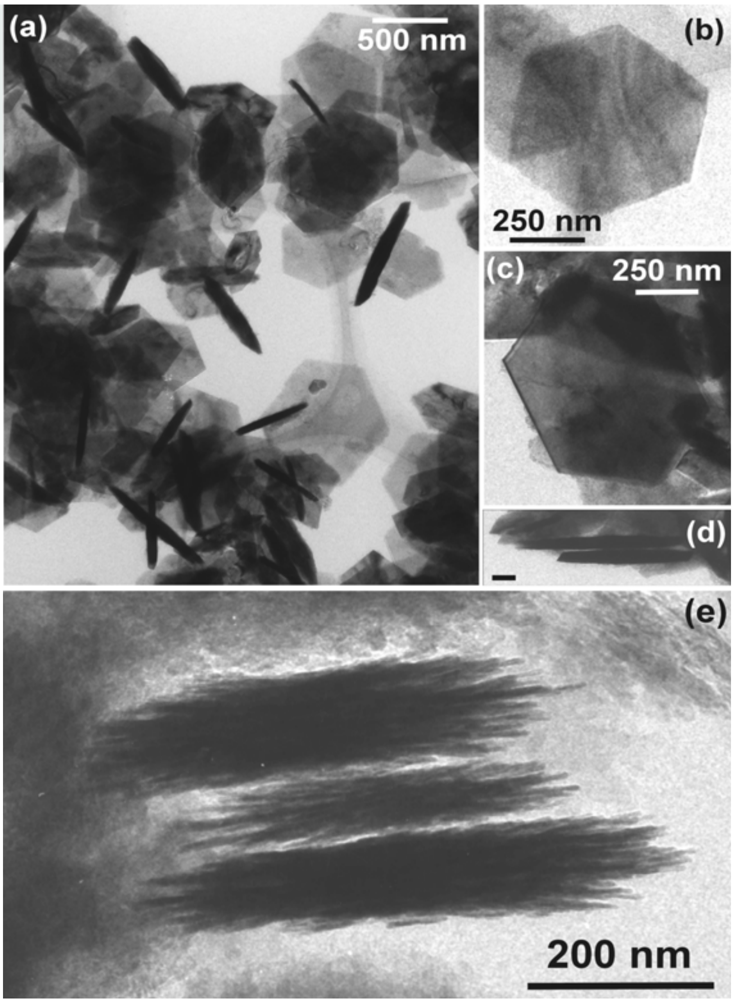

Secondary Nanopatricles

1. V_2O_5 nanofibers
2. **Coating** utilizating TEOS
3. Calcination
4. Emptying
5. SiO_2 secondary nanotubes

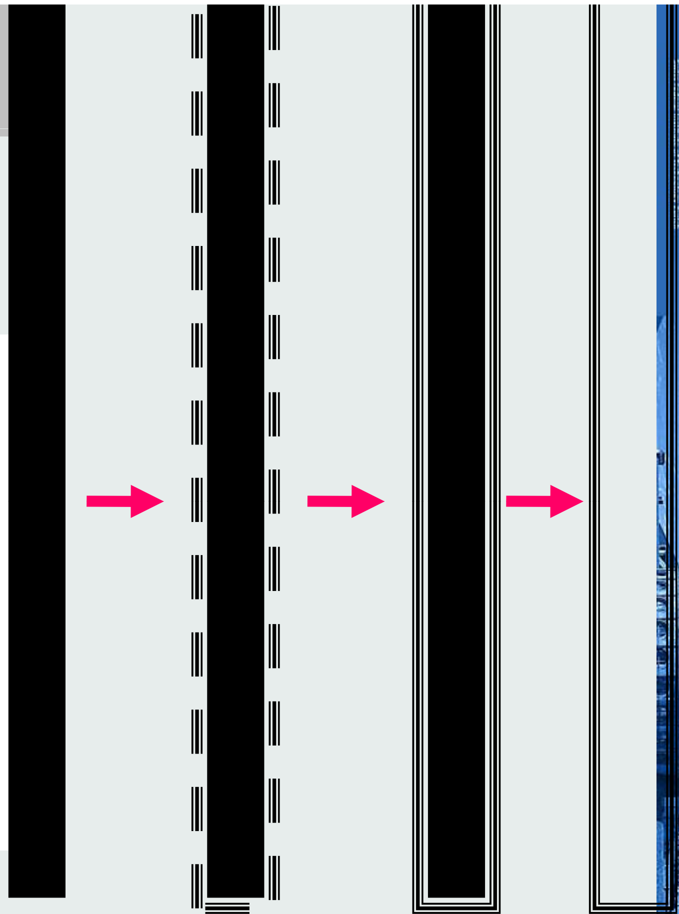

Nanotubular SiO_2

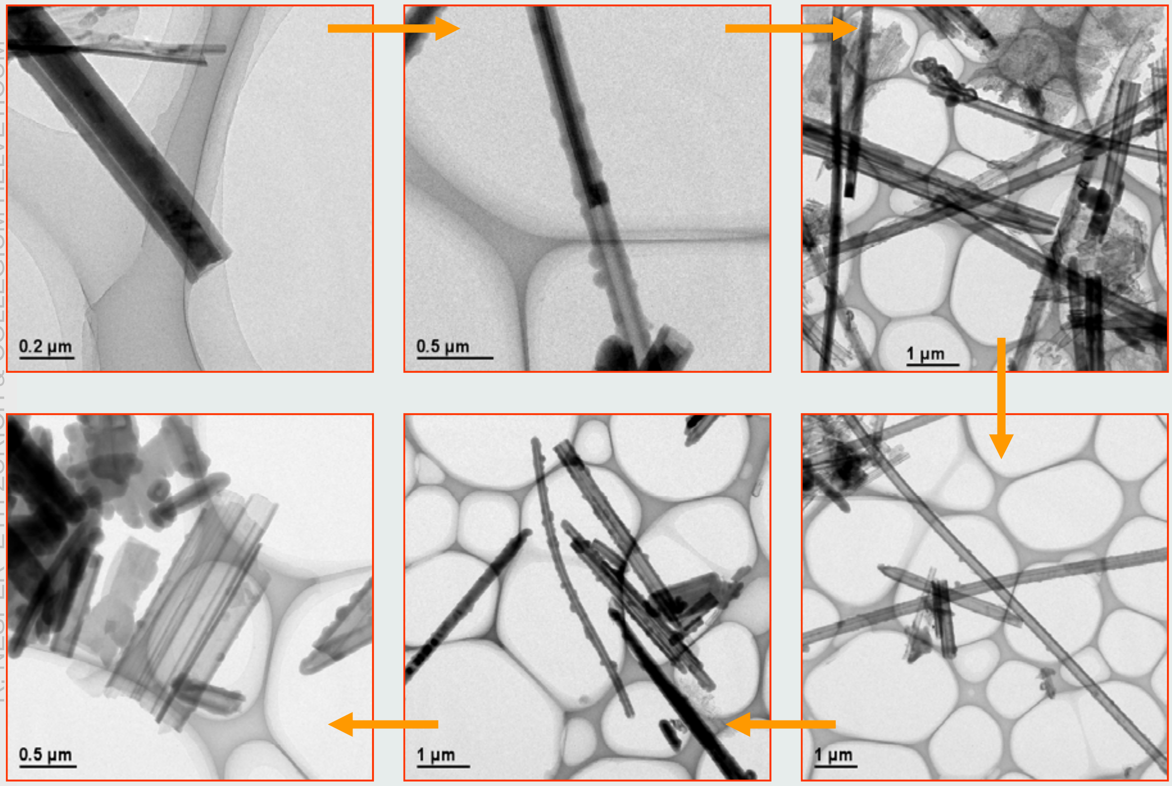

Applying Organogels

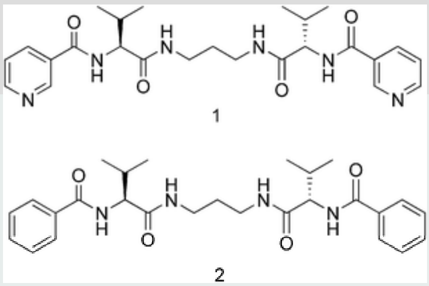

1

2

J. Mater. Chem., 2006,

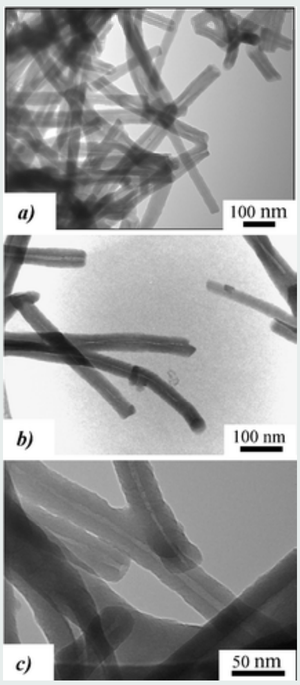

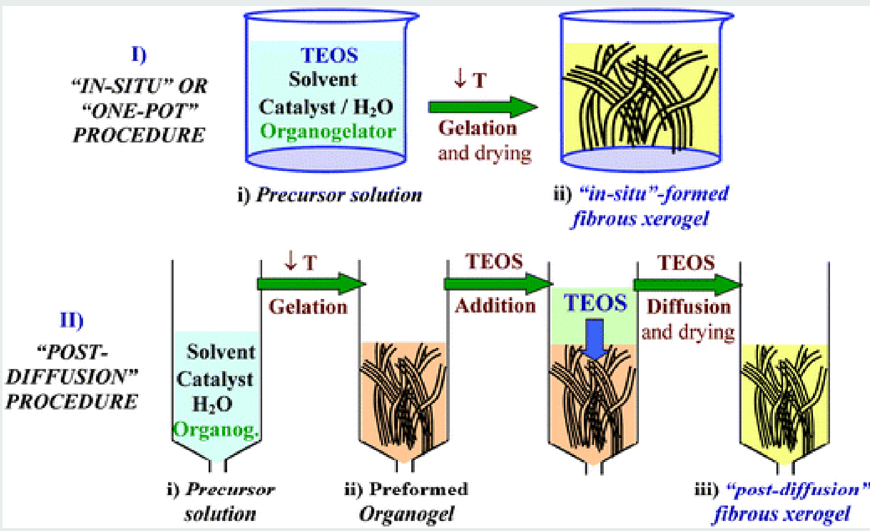

Surface Growth on Nanorods

MnO_2

on

TiO_2

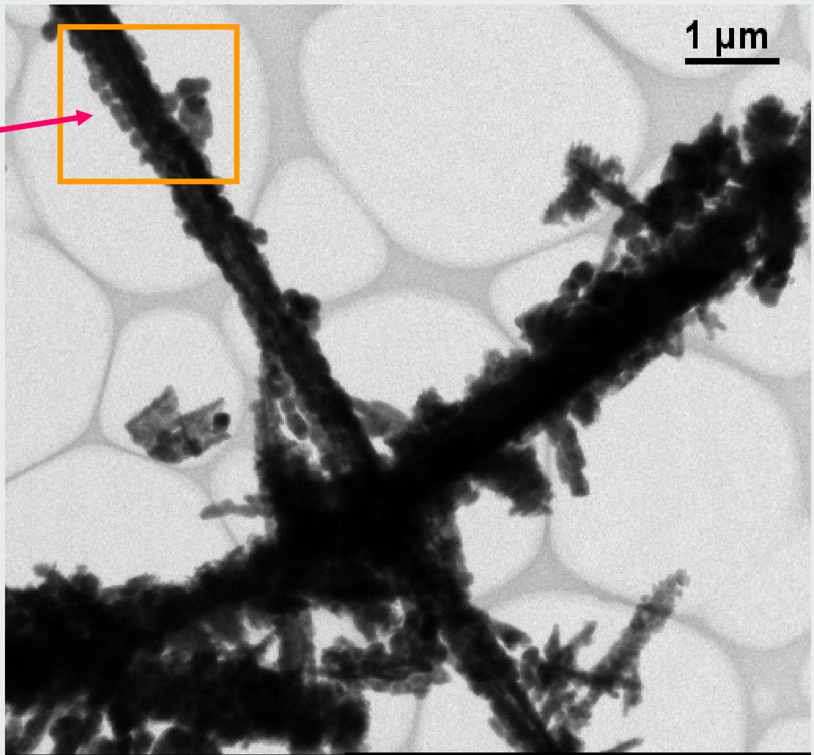

R. NESPER ETH ZÜRICH & COLLEGIUM HELVETICUM

Controlled Precursor Hydrolysis

Metal + Hydride Reaction

$$2\,Co^{2+} + 4\,BH_4^- + 9\,H_2O \rightarrow Co_2B + 12.5\,H_2 + 3\,B(OH)_3$$

Magnetic Fluids: Fabrication, Magnetic Properties, and Organization of Nanocrystals**

By *Marie-Paule Pileni**

Adv. Funct. Mater. **2001**, *11*, No. 5, October

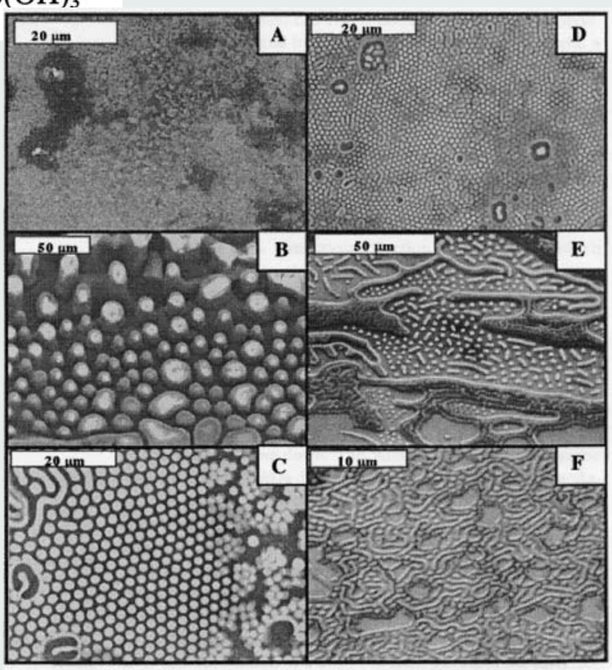

Fig. 14. SEM patterns obtained by evaporating 200 µL of a concentrated solution of cobalt nanocrystals (4×10^{-7} M in particles) deposited in a magnetic field perpendicular to the HOPG substrate. The evaporation time is 12 h. The strength of the applied field is 0 (A); 0.01 T (B); 0.27 T (C); 0.45 T (D); 0.60 T (E); and 0.78 T (F).

Applying Nano Templates

Organic Polymer Templates

R. NESPER ETH ZÜRICH & COLLEGIUM HELVETICUM

Organische Template zur Formgebung anorganischer Materialien**

*Kjeld J. C. van Bommel, Arianna Friggeri und Seiji Shinkai**

Adv. Funct. Mater. **2003**, *13*, No. 1, January

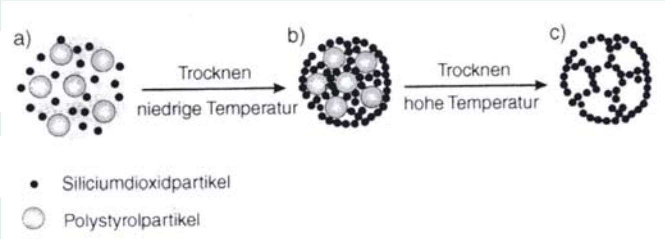

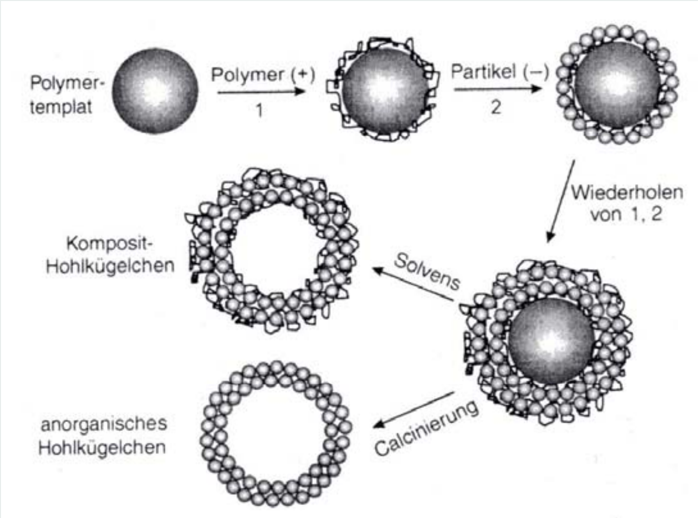

important route towards photonic crystals

Micelles/Vesicles as Nano Templates

R. NESPER ETH ZÜRICH & COLLEGIUM HELVETICUM

Emergent Nanostructures: Water-Induced Mesoscale Transformation of Surfactant-Stabilized Amorphous Calcium Carbonate Nanoparticles in Reverse Microemulsions**

By *Mei Li* and *Stephen Mann**

Nano Calcite

Bio Mineralization

Adv. Funct. Mater. **2002**, *12*, No. 11–12, D

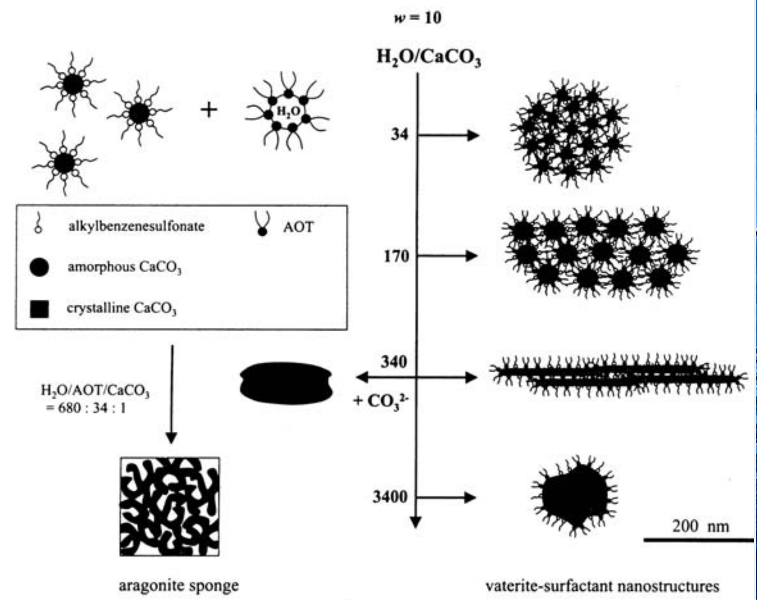

Fig. 8. General scheme showing experimental conditions and types of hybrid surfactant-vaterite nanostructures synthesized by microemulsion-mediated phase transformation of surfactant-stabilized ACC nanoparticles. Reactants are shown top/middle left. Nanostructures produced at $w = 10$ using different water droplet/amorphous $CaCO_3$ nanoparticle ratios are shown on the right. The aggregated structures are drawn approximately to scale (bar = 200 nm).

Loaded Micelles and Dendrimers

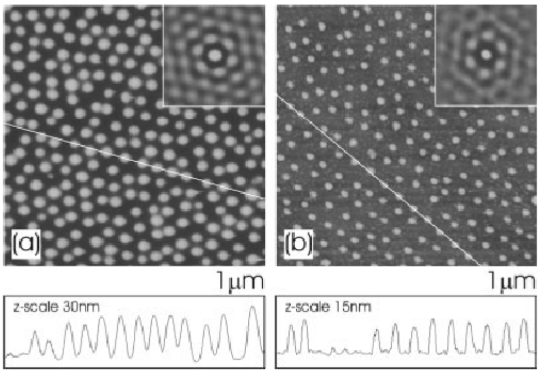

Fig. 2. Gold-loaded micelles on a silicon substrate before ((a), *z*-scale 30 nm) and after ((b), *z*-scale 15 nm) removal of the polymer matrix. Clearly, the order of the resulting nanoparticles reflects the order of the original micellar array. Local order is reasonably good as proven by the autocorrelation functions in the insets. The bottom panels show the results of line scans measured along the white lines shown.

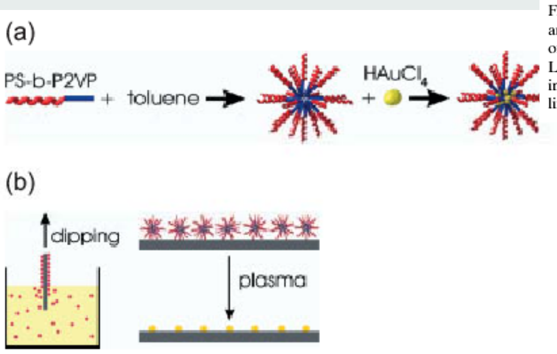

Fig. 1. a) Sketch of the formation of reverse micelles within PS-P2VP diblock copolymer solutions. The core of the micelle can be loaded with a metal precursor (e.g., $HAuCl_4$). b) The reverse micelles in solution are transferred onto substrates by dip coating. The polymer is removed and, simultaneously, the metal salt is reduced by applying either an oxygen plasma followed by a hydrogen plasma or by a single hydrogen plasma step (more details are given below).

Loaded Micelles and Dendrimers

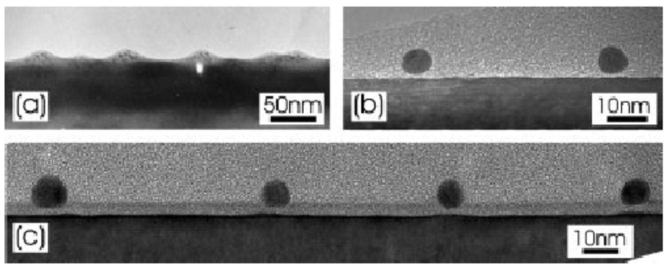

Fig. 10. TEM cross-section images of Au-salt-loaded micelles deposited onto a carbon-coated copper grid (a) and of the final array of Au nanodots prepared on top of a sapphire substrate (b) and on silicon (c), demonstrating the nearly spherical shape of the resulting particles.

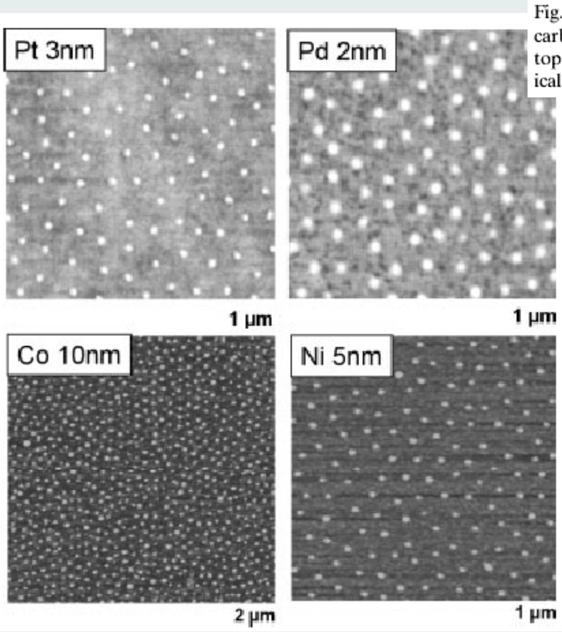

Fig. 11. AFM images of nanoparticles prepared from different elements. The universality of the micellar approach allows a wide variety of metallic, magnetic, or oxide particles to be prepared.

Silver Nanospheres from Oleic Acid Emulsions

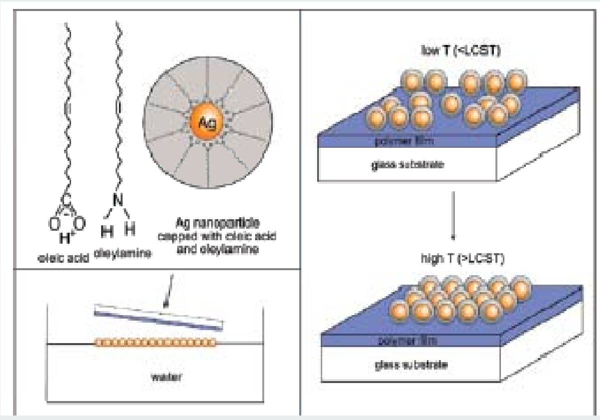

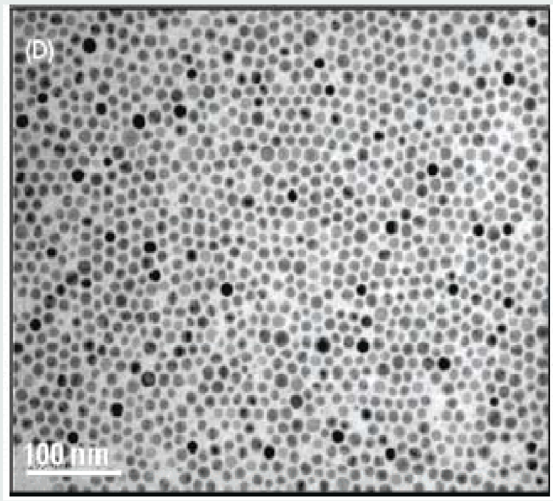

Nano Templates

R. NESPER ETH ZÜRICH & COLLEGIUM HELVETICUM

Noble-Metal Nanotubes (Pt, Pd, Ag) from Lyotropic Mixed-Surfactant Liquid-Crystal Templates**

Tsuyoshi Kijima, Takumi Yoshimura, Masafumi Uota, Takayuki Ikeda, Daisuke Fujikawa, Shinji Mouri, and Shinji Uoyama*

Angew. Chem. **2004**, 116, 230–234

Noble Metal Nano Tubes

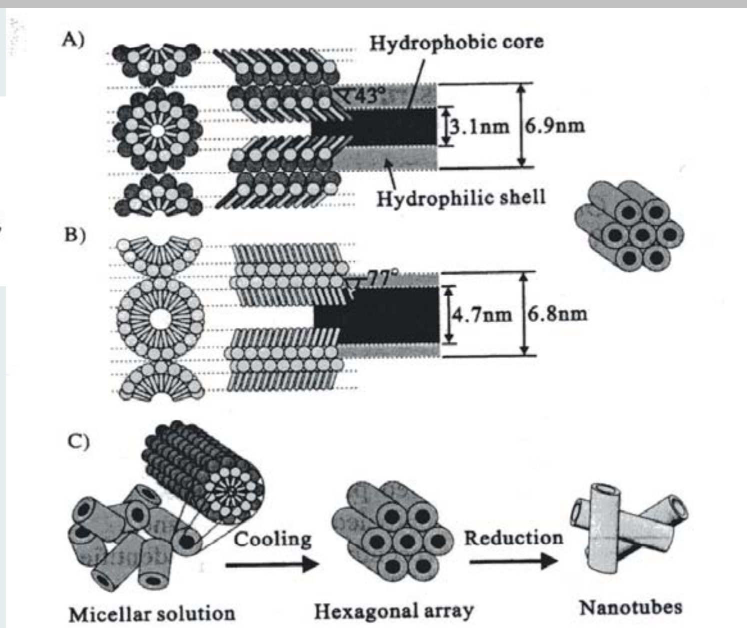

Figure 4. Schematic models for the formation of platinum nanotubes in the mixed surfactant templating system: A) Mixed ($C_{12}EO_9$/Tween 60) and B) single ($C_{12}EO_9$) surfactant cylindrical rodlike micelles. C) Pathway from micellar solution to metal nanotubes by the reduction of metals salts confined to the aqueous shell of mixed-surfactant cylindrical micelles. The metal salts and water molecules are omitted from the models.

Composite and Multimetallic Particles

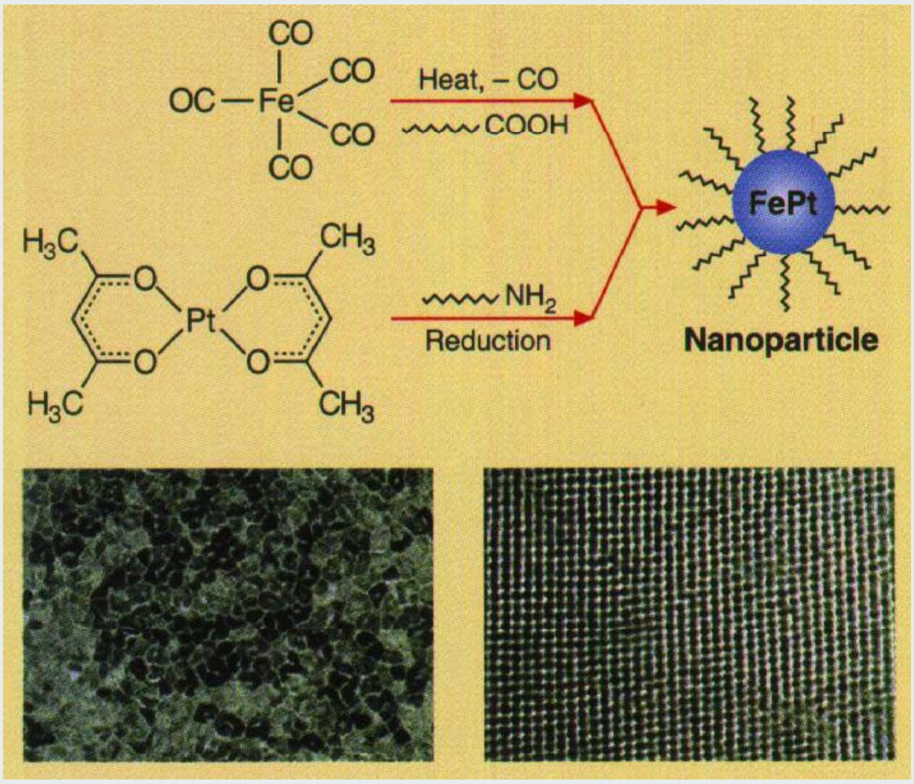

Extraction Methods

R. NESPER ETH ZÜRICH & COLLEGIUM HELVETICUM

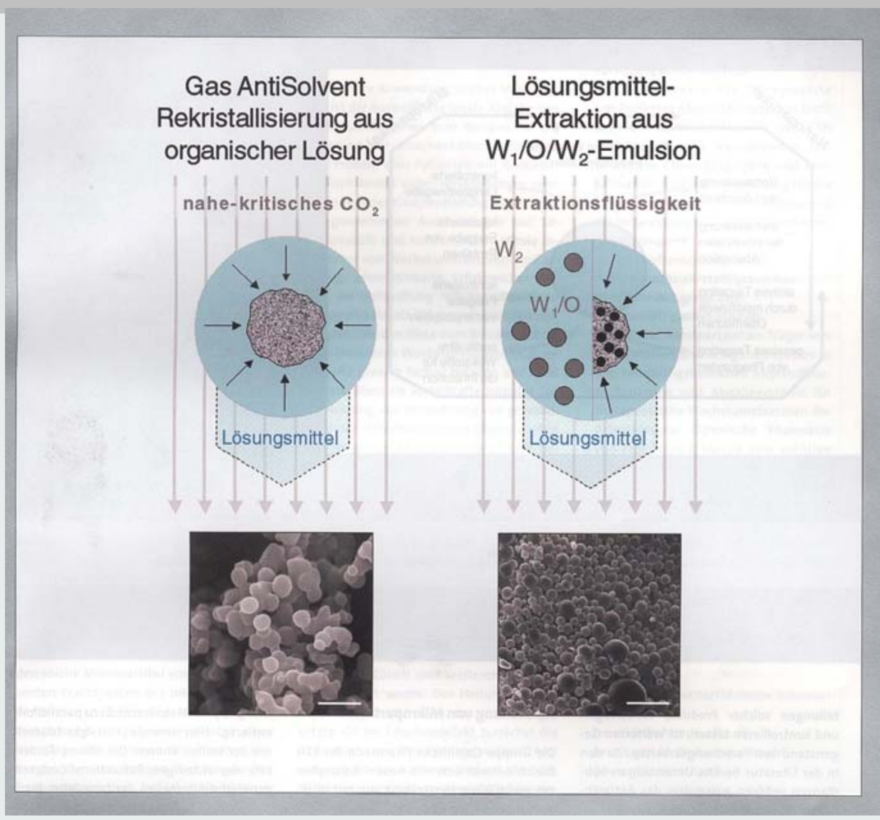

Spray Pyrolysis + Fly Ashes

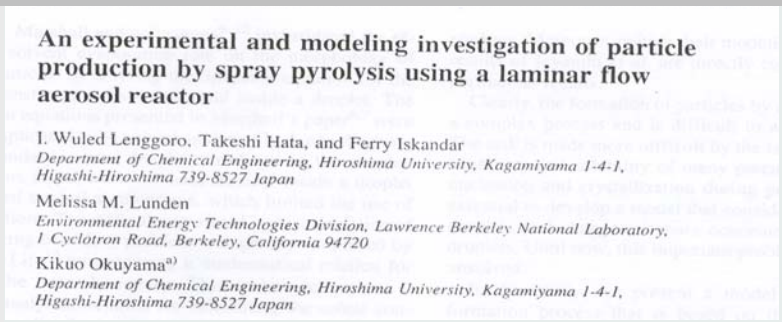

An experimental and modeling investigation of particle production by spray pyrolysis using a laminar flow aerosol reactor

I. Wuled Lenggoro, Takeshi Hata, and Ferry Iskandar
Department of Chemical Engineering, Hiroshima University, Kagamiyama 1-4-1, Higashi-Hiroshima 739-8527 Japan
Melissa M. Lunden
Environmental Energy Technologies Division, Lawrence Berkeley National Laboratory, 1 Cyclotron Road, Berkeley, California 94720
Kikuo Okuyama[a)]
Department of Chemical Engineering, Hiroshima University, Kagamiyama 1-4-1, Higashi-Hiroshima 739-8527 Japan

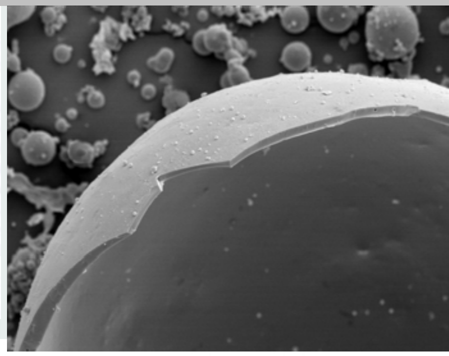

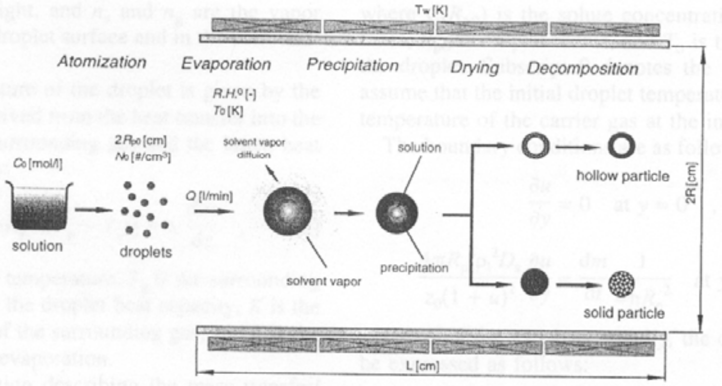

FIG. 3. Description of the simulation model.

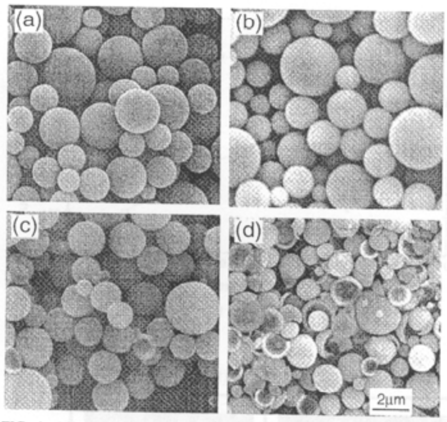

FIG. 6. Effect of furnace temperature on the morphology of zirconia particles: (a) 100 °C, (b) 200 °C, (c) 300 °C, and (d) 500 °C. Other experiment conditions: C_0 = 2 mol/l; Q = 2 l/min.

Gas Phase Reactions

Flame Synthesis

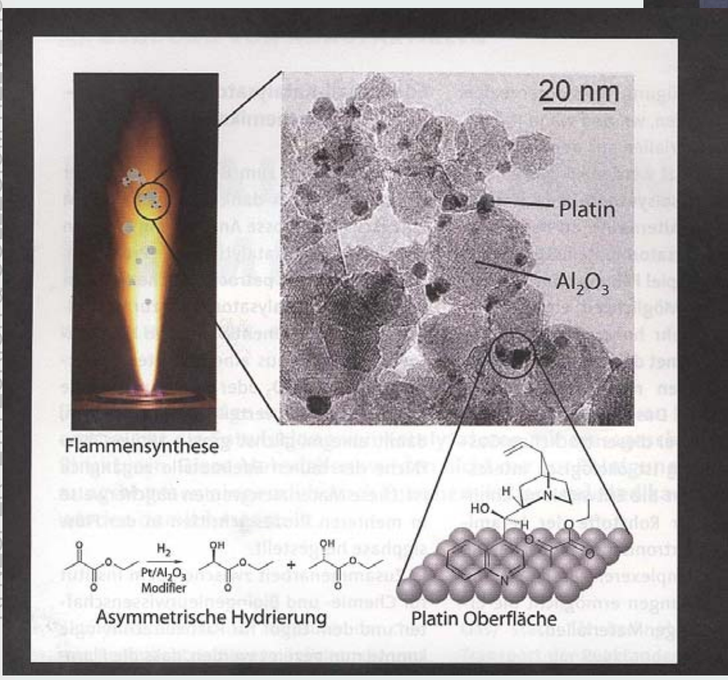

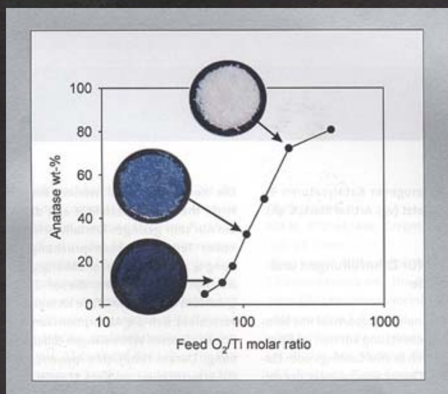

Large industrial importance

Gas Phase Reactions

Oxide Evaporation

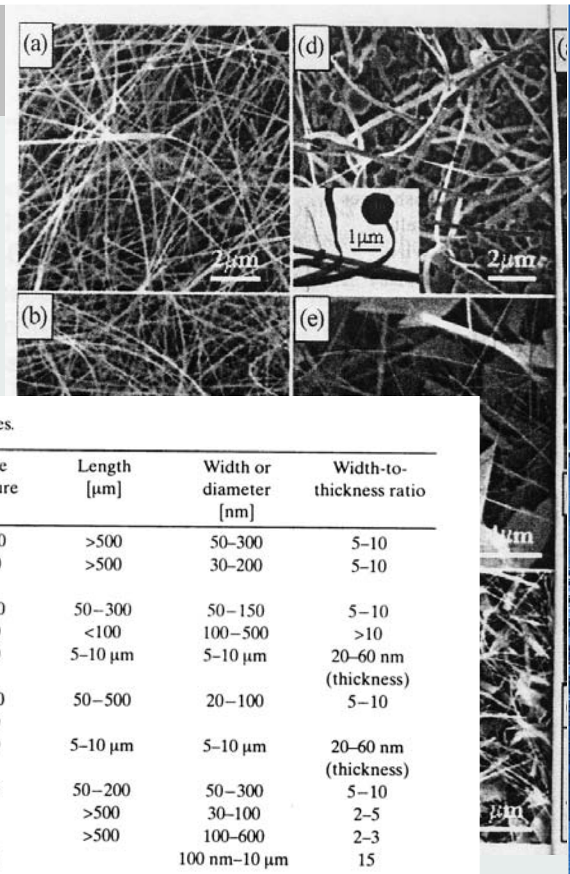

Novel Nanostructures of Functional Oxides Synthesized by Thermal Evaporation**

By *Zu Rong Dai, Zheng Wei Pan,* and *Zhong L. Wang**

Adv. Funct. Mater. **2003**, *13*, No. 1, January

Table 2. Synthesis conditions and morphology characteristics of oxide nanostructures.

Nano-structure	Source materials	Evaporation temperature [°C]	Pressure [torr]	Substrate temperature [°C]	Length [µm]	Width or diameter [nm]	Width-to-thickness ratio
ZnO belt	ZnO	1400	200–300	800–1100	>500	50–300	5–10
t-SnO_2 belt [a]	SnO	1050	200–300	800–950	>500	30–200	5–10
	SnO_2	1350					
In_2O_3 belt	In_2O_3	1400	200–300	800–1100	50–300	50–150	5–10
CdO belt	CdO	1000	200–300	700–800	<100	100–500	>10
CdO sheet	CdO	1000	200–300	700–800	5–10 µm	5–10 µm	20–60 nm (thickness)
Ga_2O_3 belt	Ga_2O_3	1400	200–300	800–1100	50–500	20–100	5–10
	GaN	950		700–850			
Ga_2O_3 sheet	GaN	950	200–300	700–850	5–10 µm	5–10 µm	20–60 nm (thickness)
PbO_2 belt	PbO	950	200–300	600–800	50–200	50–300	5–10
t-SnO_2 wire [a]	SnO	1050	250–700	25–40	>500	30–100	2–5
o-SnO_2 wire [b]	Sn+SnO	1050	200	25–40	>500	100–600	2–3
SnO diskette	SnO	1050	500–600	200–400		100 nm–10 µm	15
	SnO_2	1350					

Corrosion Methods and Phase Transitions

Porous alumina

(V, I, t, T + solv. characteristics)

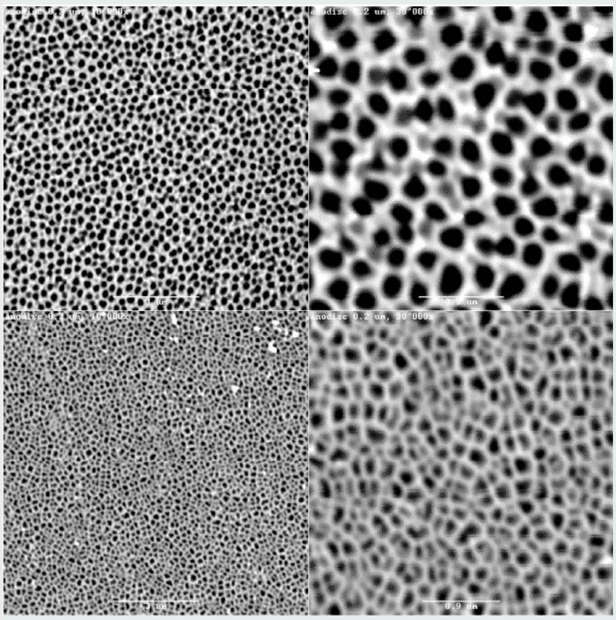

Evolution of nanoporosity in dealloying

Jonah Erlebacher*†, Michael J. Aziz*, Alain Karma‡, Nikolay Dimitrov§ & Karl Sieradzki§

Nature, 2001, 410, 450

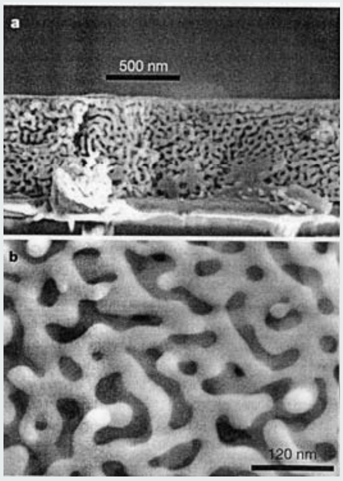

Figure 1 Scanning electron micrographs of nanoporous gold made by selective dissolution of silver from Ag-Au alloys immersed in nitric acid under free corrosion conditions. **a**, Cross-section of dealloyed $Au_{32\%}Ag_{68\%}$ (atom%) thin film. **b**, Plan view of dealloyed $Au_{26\%}Ag_{74\%}$ (atom%). The porosity is open, and the ligament spacings shown in **b** are of the order of 10 nm; spacings as small as 5 nm have been observed. Measurements of the surface area of nanoporous gold are of the order of 2 $m^2 g^{-1}$ (refs 24, 25), comparable to commercial supported catalysts.

Corrosion Methods and Phase Transitions

1. Porous alumina — anodization
2. Porous silicon — HF etching
3. Porous metals — dealloying / etching / evaporating
4. Amorphization of metals — reconstructive phase transitions, hydriding/dehydr. Precipitation (Raney metals)

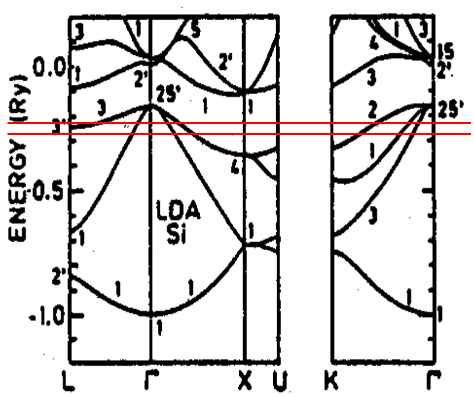

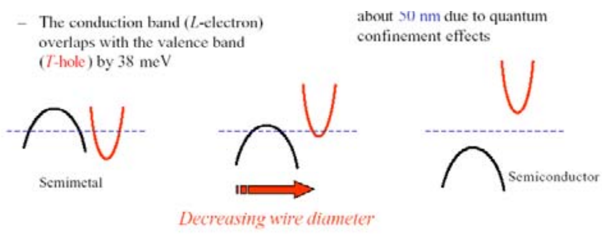

Thin films

Sputter technique

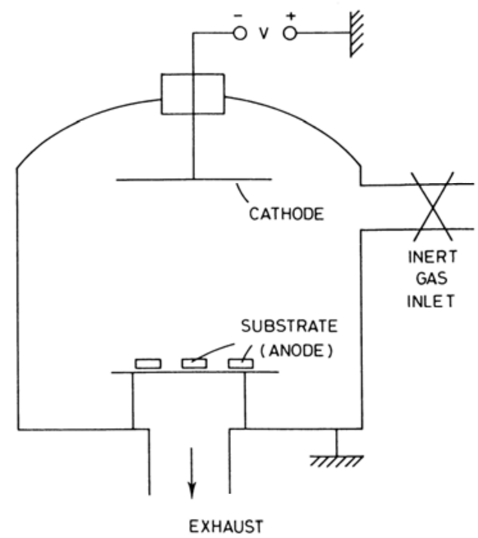

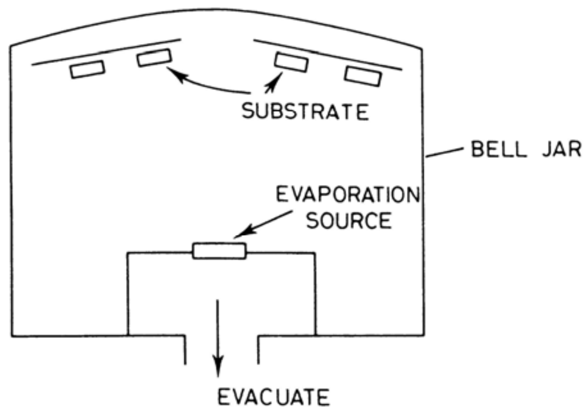

Langmuir Blodget Films

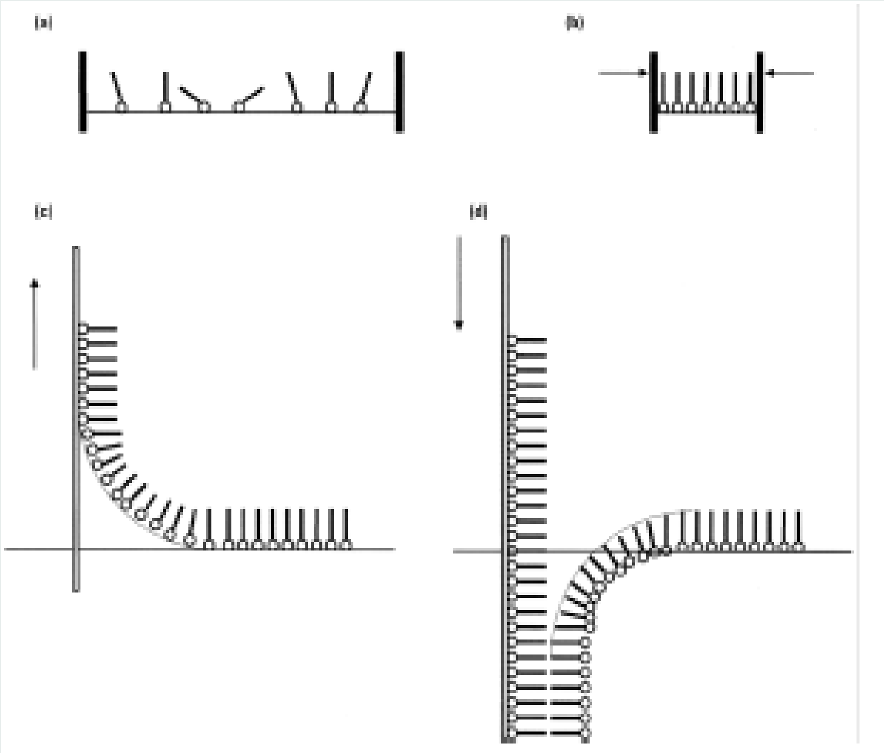

Thin Films

1. Chemical Vapor Deposition –CVD und MOCVD

$$GeH_4 \xrightarrow{\text{heat or } h\nu} Ge$$

$$Si(CH_2CH_3)_4 \xrightarrow[\text{air}]{\text{heat}} SiO_2$$

$$SiCl_4 + 2H_2 \rightarrow Si + 4HCl$$

$$SiH_4 \rightarrow Si + 2H_2$$

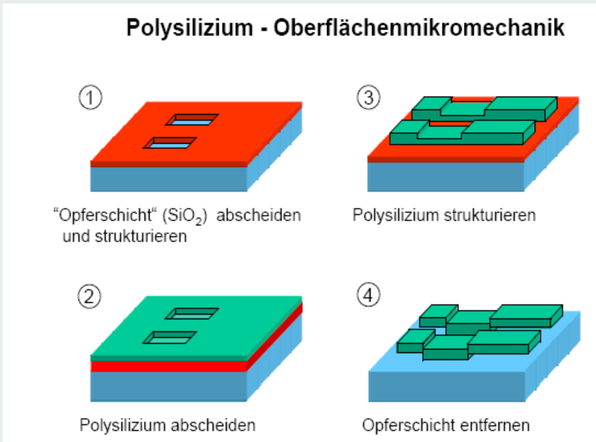

TMA ---> Trimethylaluminium $Al(CH_3)_3$
TMG ---> Trimethylgallium, $Ga(CH_3)_3$
GaAs (3-5 - semiconductor) + PH_3, AsH_3

1. **Chemical Twinning**
2. **Double Salts of Zintl Phases**
3. **Layered Compounds**
4. **Intercalated Layered Compounds**
5. **Exfoliated Layered Compounds**

S. Andersson; E. Parthe

$Ba_5Mg_{18}Si_9(Si_4)$

$Ba_6\,(Mg_{17.5}Li_{0.5})LiSi_9\,(LiSi_3)$

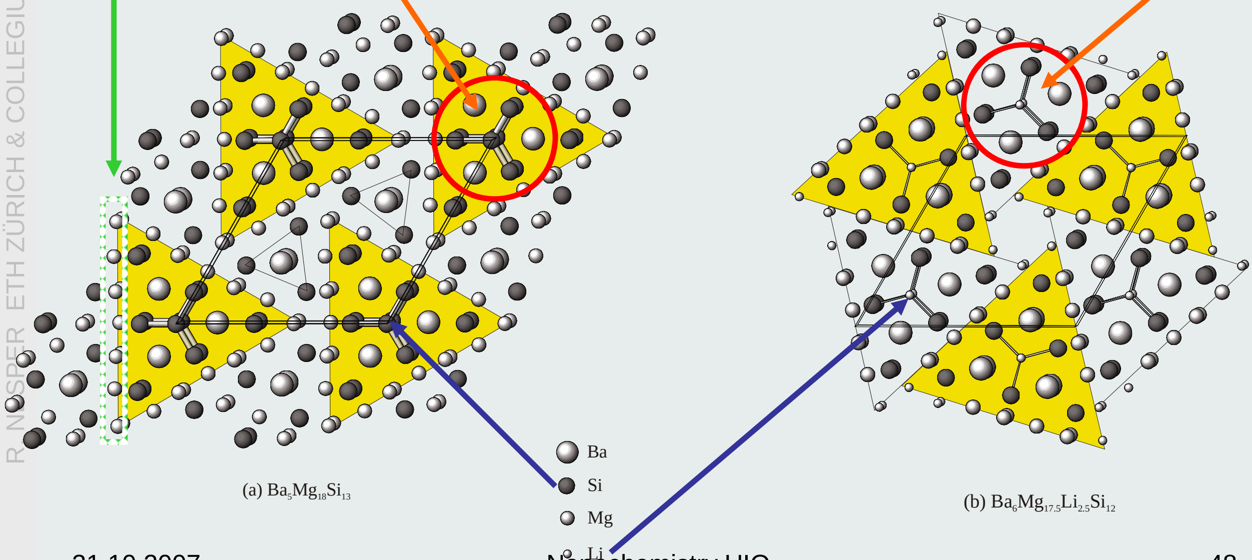

(a) $Ba_5Mg_{18}Si_{13}$

(b) $Ba_6Mg_{17.5}Li_{2.5}Si_{12}$

Double Salts - Ordered Quantum Layers

metallic

$[Ba_2Si_3]$ $[BaI_2]$

insulating

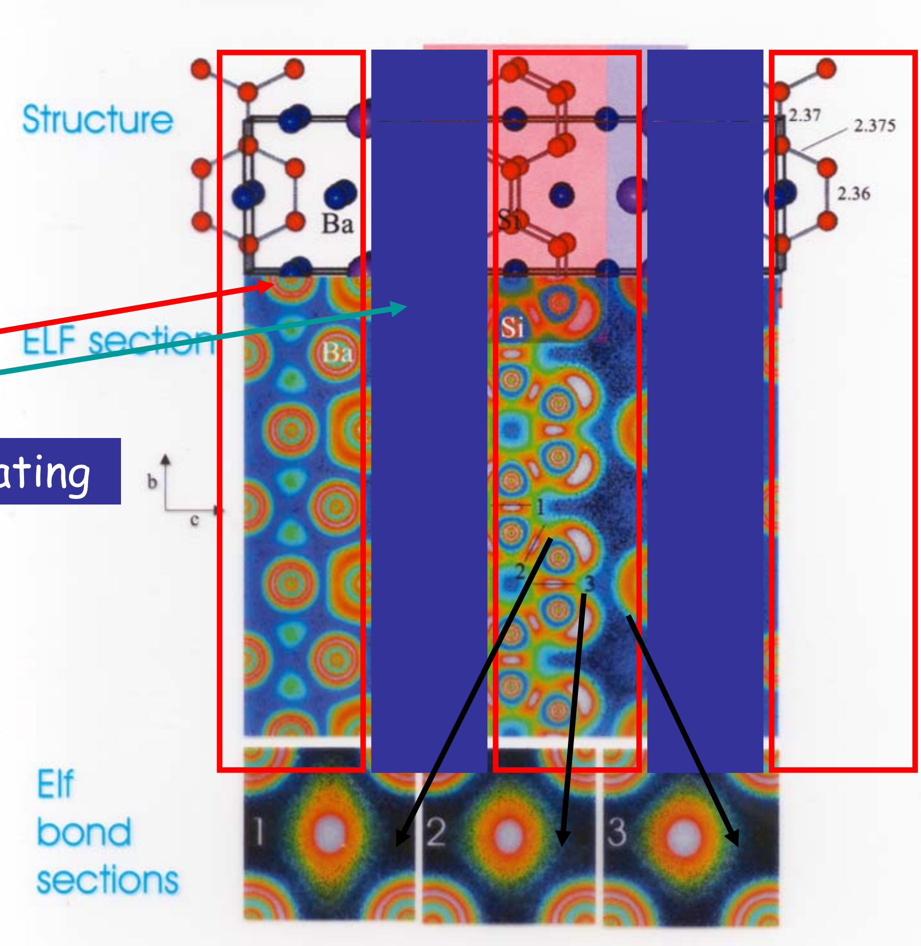

31.10.2007

R. NESPER ETH ZÜRICH & COLLEGIUM HELVETICUM